Plasma Characteristics of the Discharge Produced during Mechanoluminescence

Nathan C. Eddingsaas and Kenneth S. Suslick*

School of Chemical Sciences, University of Illinois at Urbana-Champaign, Urbana, Illinois 61801, USA

(Received 12 September 2007; published 3 December 2007)

The conditions during light emission from the fracture of solids have been difficult to determine because such mechanoluminescence (ML) is usually weak. When ML is produced by acoustic cavitation of a liquid slurry of resorcinol crystals, however, we observe bright light emission, which makes it possible to measure plasma conditions by emission spectra: a bimodal heavy atom emission temperature profile is observed with 405 ± 22 K (for 80% of emitting CH) and 4015 ± 730 K (for 20%), with an electron density and energy of $1.3 \pm 0.13 \times 10^{14}$ cm^{-3} and $\sim$3.5 eV (i.e., an effective $T_e \sim 41\,000$ K).

DOI: 10.1103/PhysRevLett.99.234301 PACS numbers: 78.60.Mq, 52.25.−b, 52.70.Kz

When a slurry of solid particles in a liquid are irradiated with ultrasound and acoustic cavitation occurs, the shock waves created in the liquid by the collapsing bubbles will accelerate the suspended particles to hundreds of meters per second, causing intense interparticle collisions [1,2]. Upon collision, the fracture of solids may give off light, i.e., mechanoluminescence (a.k.a. triboluminescence) [3–7]. When a noncentric crystal is stressed, a charge separation occurs within the crystal. Upon fracture, opposite faces of the gap will have opposing charges; the charge separation is neutralized by a dielectric breakdown of the intervening gas and of the crystal itself. Recently we have reported the increase in mechanoluminescence (ML) intensities of up to 1000-fold by the use of acoustic cavitation of slurries, and observed many new emission products not seen previously from ML, including He^+, C_2, CH, CO, and CO^+ [8,9].

While the phenomenon of ML has been know for hundreds of years [10] and the cause of the discharge is well formulated [3–5,7], the characteristics of the resultant discharge plasma have never been fully studied. Our improvement of ML intensities and the subsequent observation of new emission products now allow us to fully characterize the discharge plasma that is produced. Using well developed plasma diagnostics, we have determined the heavy atom emission temperature, electron density, and electron energy of the resulting ML discharge plasma.

Because of the small size of the discharge (within the crack), uncertainty in exact position of the discharge, and the fact that the discharge occurs in small voids in a liquid, optical emission spectroscopy has proved to be the optimal diagnostic technique. ML produces a μs to ms nonequilibrium discharge that excites the gas and vapor present at the fracture site as well as the crystal itself [3,11,12]. Because of the lack of thermodynamic equilibrium during the discharge, the gas temperature and electron temperature can be vastly different so a Maxwell-Boltzmann distribution cannot be used to determine these temperatures. Rotational relaxation of excited molecular species, however, does occur very rapidly allowing for determination of local heavy atom temperatures [13–15]. In addition, the electron density of a discharge can be determined from the Stark broadening of the Balmer lines of hydrogen [16–19]. The H_β line is most often used due to fact that it undergoes negligible self-absorption, exhibits strong Stark broadening, and is not appreciably broadened by ion dynamics; in addition, Stark broadening is mostly insensitive to temperature and so may still be applied to nonthermal plasmas. Finally, the electron temperature can be determined from the ratio of the intensities of spectral lines of the same element when the energy separation between the lines is greater than the electron energy; for example, lines from the subsequent ionization states of He have been used to determine electron energies from 2–11 eV [20,21].

In order to apply plasma diagnostics to the ML discharge, we require an estimate of the pressure of the gas within the fracture site. To do this, first the rate of fracture and duration of a ML event was calculated [11,12], and then gas diffusion into the resulting void was determined using Fick's Law of mass diffusion, which describes the transport of dissolved gas within a liquid. A reasonable estimate as to the pressure of gas within the fracture site during the discharge event is $\sim$0.1 bar. We also assume that for these slurries in low volatile liquids (e.g., dodecane), He is the major gas component by a wide margin, so collisions with other species may be ignored. Finally, we assume that the resulting plasma is optically thin for all emitting species, a reasonable assumption given the low density and small size of the plasma and confirmed by the absence of any unaccounted broadening or flattening of spectral lines.

The ML discharge is nonthermal, so heavy atom temperatures cannot be determined by Maxwell-Boltzmann distributions. Vibrational and rotational collisional transfer, moreover, results in partial thermalization of the rotational excited state population before electronic quenching or emission occurs [13,22–24]. The rate constant for rotational energy transfer of CH ($A^2\Delta$), with He as the collision partner, is 1.3×10^{-10} cm^3 s^{-1}, much faster than the radiative lifetime of 538 ns [25].

Figure 1(a) shows the CH ($A^2\Delta - X^2\Pi$) emission from ML of resorcinol, together with the simulated CH spectrum. The ML spectrum was obtained by ultrasonic irradiation (6 W/cm^2 at 20 kHz) of a slurry of resorcinol crystals in liquid dodecane at 300 K sparged with He. This acoustic intensity is roughly tenfold less than that typically used for sonochemical or sonoluminescence experiments, and no direct sonoluminescence is observed under these conditions from dodecane. More detailed experimental procedures can be found in previous reports [8,9].

In Fig. 1(b) is the semilogarithmic plot of the rotational population versus the rotational energy determined from the simulated spectrum, as well as best fit lines to the data. As can be seen, the rotational population can be well fit to a bimodal distribution of temperatures, $T_{r1} = 405 \pm 22$ K, which represents 80% of the emitting CH, and $T_{r2} = 4015 \pm 730$ K, which represents the remaining 20%. This bimodal distribution arises from the fact that high rotational quantum numbers have spacings much larger than the thermal collision energy, so many more collisions are necessary for full thermal relaxation, resulting in emission from CH still hot after formation by electron impact on hydrocarbon vapor. The larger error in the high temperature T_{r2} arises in part from the fact that >80% of the rotational population is in the thermalized state and in part from the wide distribution of hot CH that T_{r2} actually represents. Similar bimodal populations of rotational levels of CH have been observed in electric discharges of alkanes at pressures from a few mbar up to an atmosphere [13,22,26].

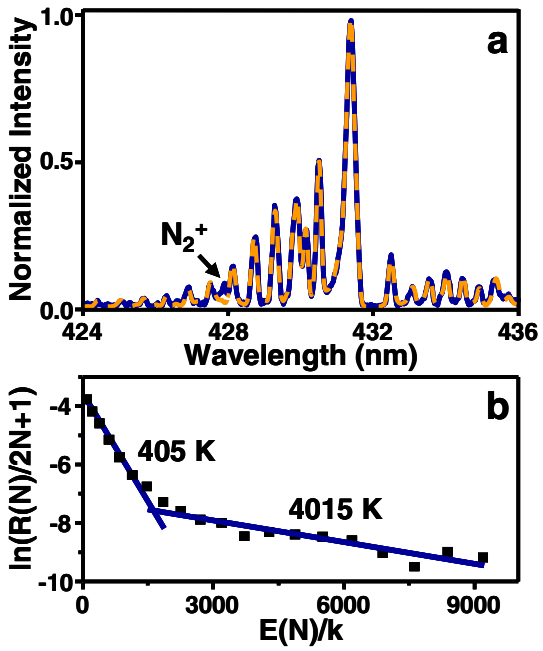

FIG. 1 (color online). (a) Mechanoluminescence of CH ($A^2\Delta - X^2\Pi$) from sonication of resorcinol crystals in a dodecane slurry at 300 K sparged with He: observed ML (—) and simulated spectrum (dashed line). (b) Boltzmann plot of rotational distribution and bimodal fit (—); $T_{r1} = 405 \pm 22$ K, $T_{r2} = 4015 \pm 730$ K.

As shown in Fig. 2, the high resolution spectrum of the resorcinol ML in dodecane sparged with He contains the H_β line as well as the He I $4^1D - 2^1P$ and $4^1F - 2^1P$ transitions, which were used to determine the electron density during the ML discharge. As long as the electron density is greater than $\sim 5 \times 10^{13}$ cm^{-3}, the electron number density can be determined from the broadening of the H_β line at 486.1 nm. The excited state H atoms in this system result from the discharge through H_2, CH_4, and C_2H_2 (sonolysis products of dodecane [9,27]), so no external H_2 source needed to be added. The line shape of the H_β line is a convolution of the Gaussian (instrument, Doppler) and Lorentzian (natural, resonance, van der Waals, Stark) broadening mechanisms resulting in a Voigt profile [14–16,18]. The full width at half maximum (FWHM) of the Gaussian component ($\Delta\lambda_G$) is given by

$$\Delta\lambda_G = (\Delta\lambda_{\text{inst}}^2 + \Delta\lambda_{\text{Dopp}}^2)^{1/2}, \quad (1)$$

while the FWHM of the Lorentzian component ($\Delta\lambda_L$) is a linear combination of its parts:

$$\Delta\lambda_L = \Delta\lambda_{\text{nat}} + \Delta\lambda_{\text{res}} + \Delta\lambda_{\text{VdW}} + \Delta\lambda_{\text{Stark}}, \quad (2)$$

and the two can be combined together to get the Voigt FWHM ($\Delta\lambda_V$) using the method derived by Whiting [28]:

$$\Delta\lambda_V = \frac{\Delta\lambda_L}{2} + \sqrt{\left(\frac{\Delta\lambda_L^2}{4} + \Delta\lambda_G^2\right)}. \quad (3)$$

The instrument broadening was 0.34 Å, as determined from the Gaussian profile of lines from a Hg-Ar pen lamp.

The other components of the broadening are derived mathematically from well established plasma diagnostics [14–20]. Doppler broadening is caused by thermal move-

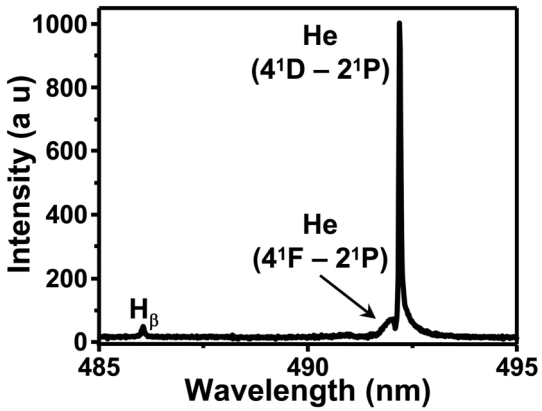

FIG. 2. High resolution spectrum used to determine the electron density of mechanoluminescence from sonication of resorcinol crystals in a dodecane slurry sparged with He. The spectrum consists of He I ($4^1D - 2^1P$) transition, the forbidden He I ($4^1F - 2^1P$) transition, and the H_β line at 486.1 nm.

ment of an atom relative to the observer resulting in an apparent shift in the frequency of the emission. The FWHM of the Doppler broadening can be expressed [14] by

$$\Delta\lambda_{\mathrm{Dopp}} = 7.16 \times 10^{-7}\lambda\sqrt{\frac{T_0}{M}}, \quad (4)$$

where λ is the wavelength in Å, T_0 is the temperature of the emitter in K, and M is the atomic weight of the emitter. Using the gas temperature determined by the CH $(A - X)$ emission, the $\Delta\lambda_{\mathrm{Dopp}}$ is found to be 0.070 Å.

Natural broadening is a result of the uncertainty in the energy of the states involved in the transition and is important in Mössbauer nuclear spectroscopy, but rarely in atomic electronic spectra. The FWHM of the natural broadening of the H_β line is 6.2×10^{-5} Å and can be safely ignored.

Resonance broadening is a result of collisions between like particles, i.e., two hydrogen atoms colliding with each other. Resonance broadening is dependent both on the total pressure in the system and the mole fraction of the emitter within the system. As argued earlier, the total pressure during discharge is <0.1 bar and only a small fraction of the gas will be hydrogen, so collisions between H atoms will be infrequent. The amount of broadening due to resonance broadening in this system will be negligible, even less than natural broadening.

van der Waals broadening is a result of collisions with neutral perturbers that do not share a resonant transition with the emitter. Under conditions of H atoms interacting with He, the equation for the FWHM of the van der Waals broadening [14] can be represented as

$$\Delta\lambda_{\mathrm{vdW}} = 4.09 \times 10^{-13}\lambda^2(\bar{\alpha}\bar{R}^2)^{2/5}\left(\frac{T_g}{\mu}\right)^{3/10} n_{\mathrm{He}}, \quad (5)$$

where λ is the wavelength in Å, $\bar{\alpha}$ is the average polarizability of the neutral perturber (for He, this is $1.38 \times a_0^3$, where a_0 is the Bohr radius in cm), $\bar{R}^2 \approx 600 \times a_0^2$, which is derived from the ionization energy of H and the energy levels of the H_β transition, T_g is the gas temperature in K, μ is the reduced mass of the emitter-perturber system, and n_{He} is the neutral He gas density in cm^{-3}. Under the conditions of the ML discharge, the $\Delta\lambda_{\mathrm{vdW}}$ is 0.047 Å.

Stark broadening is a result of Coulombic interactions between the radiating species and the charged particles present in the plasma. Both electrons and ions induce Stark broadening, but the electron contribution dominates due to their higher relative velocity. The Stark effect on the H_β line has been well studied and the broadening parameters have been well developed. The FWHM (in Å) for Stark broadening can be represented [14] by

$$\Delta\lambda_{\mathrm{Stark}} = 2.0 \times 10^{-10} n_e^{2/3}, \quad (6)$$

where n_e is the electron density in cm^{-3}.

Figure 3 gives a high resolution spectrum of the H_β line observed during ML, the Voigt fit (FWHM 0.72 Å), and the instrumental broadening. Since the contribution to the line width from the other broadening mechanisms is known, the portion of the FWHM due to the Stark effect can be determined using Eq. (1)–(3) and is found to be 0.55 Å. Using Eq. (6) the electron density is found to be $1.3 \pm 0.13 \times 10^{14}$ cm^{-3}. The H_β linewidth is highly sensitive to the electron density: for comparison, the calculated Stark linewidth would be 0.41 Å at an electron density of 10^{14} cm^{-3} and 1.97 Å at 10^{15} cm^{-3} [16,17].

Another indicator of electron density is the presence of the $4^1F - 2^1P$ forbidden transition near the $4^1D - 2^1P$ transition of He at 492.2 nm; emission from this forbidden transition is induced by the electric microfield in the plasma which causes a breakdown of the parity selection rule [29–31]. The blue shift and intensity of the forbidden component relative to the He line at 492.2 nm is strongly dependent on electron density. Figure 2 shows the He $(4^1D - 2^1P)$ along with the forbidden component $(4^1F - 2^1P)$ observed during ML. By comparing the position and intensity of this line to that previously reported, we can estimate semiquantitatively an electron density between 10^{14} and 10^{15} cm^{-3}, which is fully consistent with the value determined by the H_β line.

At high electron densities ($n_e > 10^{18}$ cm^{-3}), line ratios will adhere to the Saha-Boltzmann formula, and the electrons will be in thermodynamic equilibrium. At lower densities, thermodynamic equilibrium is not reached, but the electron energy can be determined by comparing intensities of emission lines from excited states of suitably large energy difference of the same element, such as the He I line at 587.6 nm and the He II line at 468.6 nm [20,21]. Mewe expanded on the work of Griem to determine the electron temperature based on the ratio of these two lines using the equation

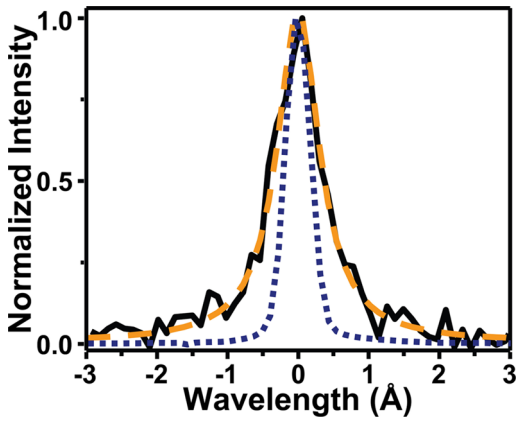

FIG. 3 (color online). H_β line from ML of resorcinol in dodecane sparged with He: ML (—), Voigt fit (FWHM: 0.718 Å) (dashed line), and instrumental broadening (FWHM: 0.342 Å) (dotted line).

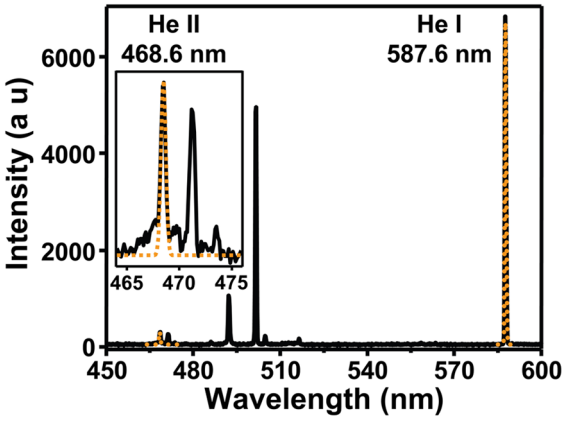

FIG. 4 (color online). Comparison of the He I (587.6 nm) and He II (468.6 nm) emission lines produced from ML of resorcinol in dodecane sparged with He: ML (—), Gaussian fit (dashed line). The ratio of area of the HeII/HeI line is 0.035.

$$\frac{I_a}{I_b} = 6 \times 10^{21} \frac{(gf/\lambda^3)_a}{(gf/\lambda^3)_b} \frac{b_p{}^{(1)}}{b_q{}^{(0)}} \frac{1}{b_1{}^{(1)} n_e} (kT_e)^{3/2} \times \exp\left\{\frac{54.4}{kT_e}\left(\frac{1}{p^2} - \frac{1}{4q^2} - 1\right)\right\}, \quad (7)$$

where g is the statistical weight, f is the absorption oscillator strength, λ is the wavelength of the line in Å, $b_p{}^{(z)}$ is the ratio between rates of collisional ionization and recombination to level p (constants found in Ref. [21]), n_e is the electron density in cm^{-3}, and kT_e is the electron energy in eV.

Figure 4 shows the ML from resorcinol in dodecane sparged with He along with Gaussian fits to the He I line at 587.6 nm and the He II line at 468.6 nm. From these fits it was found that the $\mathrm{HeII}_{468.6}/\mathrm{HeI}_{587.6}$ ratio is 3.5×10^{-2}, which corresponds to an electron energy of 3.5 eV (i.e., an effective $T_e \sim 41\,000$ K). Because our gas pressure is near the lower limit for the applicability of Eq. (7), the electron energy estimate is a lower limit [21]. It should also be noted that ML discharge is *not* well represented by a steady-state corona discharge model, where collisional ionization or excitation is in balance with radiative recombination or spontaneous decay; the steady-state model would require an electron energy of >1 keV for the low electron densities present during ML.

In summary, optical emission spectroscopy was used to characterize the mechanoluminescence discharge in terms of heavy atom temperature, electron density, and electron energy. A bimodal heavy atom emission temperature profile is observed with 405 ± 22 K (80% of emitting CH) and 4015 ± 730 K (20%), with an electron density of $1.3 \pm 0.13 \times 10^{14}$ cm^{-3}, and electron energy of ~3.5 eV (i.e., an effective $T_e \sim 41\,000$ K). These results are very similar to other microdischarges such as direct current microplasmas [15], microplasma jets [14], and dielectric barrier discharges [13,32,33]. All of these microplasmas create highly reactive environments and have applications for remediation of chemical toxins, sterilization, surface treatment, lighting, and ozone production.

*ksuslick@uiuc.edu

[1] S. J. Doktycz and K. S. Suslick, Science **247**, 1067 (1990).
[2] T. Prozorov, R. Prozorov, and K. S. Suslick, J. Am. Chem. Soc. **126**, 13 890 (2004).
[3] A. J. Walton, Adv. Phys. **26**, 887 (1977).
[4] J. I. Zink, Naturwissenschaften **68**, 507 (1981).
[5] L. M. Sweeting, Chem. Mater. **13**, 854 (2001).
[6] I. Sage and G. Bourhill, J. Mater. Chem. **11**, 231 (2001).
[7] B. P. Chandra, in *Luminescence of Solids*, edited by D. R. Vij (Plenum, New York, 1998), p. 361.
[8] N. C. Eddingsaas and K. S. Suslick, Nature (London) **444**, 163 (2006).
[9] N. C. Eddingsaas and K. S. Suslick, J. Am. Chem. Soc. **129**, 6718 (2007).
[10] F. Bacon, *Of the Advancement of Learning* (J. M. Dent and Sons, London, 1915).
[11] B. P. Chandra and J. I. Zink, J. Chem. Phys. **73**, 5933 (1980).
[12] B. P. Chandra, J. Phys. D: Appl. Phys. **10**, 1531 (1977).
[13] J. Luque *et al.*, J. Appl. Phys. **93**, 4432 (2003).
[14] A. Yanguas-Gil *et al.*, J. Appl. Phys. **101**, 103307 (2007).
[15] Q. Wang *et al.*, J. Phys. D: Appl. Phys. **38**, 1690 (2005).
[16] H. R. Griem, *Spectral Line Broadening by Plasmas* (Academic, New York, 1974).
[17] P. Kepple and H. R. Griem, Phys. Rev. **173**, 317 (1968).
[18] C. O. Laux *et al.*, Plasma Sources Sci. Technol. **12**, 125 (2003).
[19] C. Yubero, M. D. Calzada, and M. C. Garcia, J. Phys. Soc. Jpn. **74**, 2249 (2005).
[20] H. R. Griem, *Plasma Spectroscopy* (Mc-Graw Hill, New York, 1964).
[21] R. Mewe, Br. J. Appl. Phys. **18**, 107 (1967).
[22] J. L. Cooper and J. C. Whitehead, J. Chem. Soc., Faraday Trans. **89**, 1287 (1993).
[23] W. Brennen and T. Carrington, J. Chem. Phys. **46**, 7 (1967).
[24] R. N. Dixon, D. P. Newton, and H. Rieley, J. Chem. Soc., Faraday Trans. 2 **83**, 675 (1987).
[25] K. H. Becker, H. H. Brenig, and T. Tatarczyk, Chem. Phys. Lett. **71**, 242 (1980).
[26] T. Nagata *et al.*, Chem. Phys. **88**, 163 (1984).
[27] K. S. Suslick *et al.*, J. Phys. Chem. **87**, 2299 (1983).
[28] E. E. Whiting, J. Quant. Spectrosc. Radiat. Transfer **8**, 1379 (1968).
[29] D. D. Burgess and C. J. Cairns, J. Phys. B **4**, 1364 (1971).
[30] T. Schoening, J. Phys. B **27**, 4501 (1994).
[31] A. J. Barnard, J. Cooper, and E. W. Smith, J. Quant. Spectrosc. Radiat. Transfer **15**, 429 (1975).
[32] X. Xu, Thin Solid Films **390**, 237 (2001).
[33] U. Kogelschatz, B. Eliasson, and W. Egli, Pure Appl. Chem. **71**, 1819 (1999).